Atmos. Meas. Tech. Discuss., doi:10.5194/amt-2016-233, 2016
Manuscript under review for journal Atmos. Meas. Tech.
Published: 1 September 2016

Atmospheric Measurement Techniques Discussions

Retrieval of nitric oxide in the mesosphere from SCIAMACHY nominal limb spectra

Stefan Bender[1], Miriam Sinnhuber[1], Martin Langowski[2], and John P. Burrows[3]

[1]Karlsruhe Institute of Technology, Karlsruhe, Germany
[2]Ernst–Moritz–Arndt–University, Greifswald, Germany
[3]University of Bremen, Bremen, Germany

Correspondence to: S. Bender
(stefan.bender@kit.edu)

Abstract. We retrieve nitric monoxide (NO) number densities from measurements from the SCanning Imaging Absorption spectroMeter for Atmospheric CHartographY (SCIAMACHY, on Envisat) nominal limb mode (0–91 km). We derive the NO number densities from atmospheric emissions in the gamma bands in the range 230–300 nm, measured by the SCIAMACHY ultra-violet (UV) channel 1. We adapt the NO retrieval from the mesosphere and lower thermosphere mode (MLT, 50–150 km) (Bender et al., 2013), including the same 3-D ray tracing, 2-D retrieval grid, and regularisations with respect to altitude and latitude.

Since the nominal mode limb scans extend only to about 91 km, we use NO densities in the lower thermosphere (above 92 km) derived from empirical models as a priori input. As priors we use the NOEM model (Marsh et al., 2004) and a regression model derived from the MLT NO data comparison (Bender et al., 2015). Our algorithm yields meaningful NO number densities from 60 km to 85 km from the SCIAMACHY nominal limb mode scans. Using a priori input substantially reduces the misidentification of NO from the lower thermosphere, where no direct limb measurements are available. We achieve a vertical resolution of 5–10 km in the altitude range 65–80 km.

Analysing all SCIAMACHY nominal limb scans provides almost ten years (from August 2002 to April 2012) of daily NO measurements in this altitude range. This provides a unique data record of NO in the upper atmosphere and is invaluable to constrain NO in the mesosphere, in particular for testing and validating chemistry climate models during this period.

1 Introduction

Solar, auroral, and radiation belt electrons as well as soft solar X-rays produce nitric monoxide (NO) in the mesosphere and lower thermosphere (MLT, 50–150 km). Hence, the NO content in this atmospheric region reveals how solar and geomagnetic activity and variability impact the atmospheric composition (Hendrickx et al., 2015; Sinnhuber et al., 2016). NO downward transport during polar winters then influences the lower atmosphere, in particular by catalytically reducing stratospheric ozone (Sinnhuber et al., 2012; Seppälä et al., 2015; Verronen and Lehmann, 2015). This in turn changes the heating and cooling and eventually the atmospheric circulation, possibly down to tropospheric weather systems as supported by observations (Seppälä et al., 2009; Maliniemi et al., 2014). Therefore, NO data from the mesosphere are crucial to link solar and geomagnetic activity to atmospheric composition and dynamics.

Atmos. Meas. Tech. Discuss., doi:10.5194/amt-2016-233, 2016
Manuscript under review for journal Atmos. Meas. Tech.
Published: 1 September 2016

Atmospheric Measurement Techniques Discussions

We adapt the NO retrieval for the SCIAMACHY MLT limb mode (Bender et al., 2013) to the nominal limb scans. Since the nominal scans are carried out only up to about 91 km, direct measurements of the lower thermosphere are missing. However, these are needed to exactly quantify the NO content above 100 km, where the maximal density is located (Barth et al., 2003; Marsh et al., 2004; Minschwaner et al., 2004; Funke et al., 2005; Bender et al., 2015). The instrument observes the whole emission along the line of sight, including the NO layer in the lower thermosphere. But because the nominal limb scans have no tangent points above 91 km, the retrieval maps these enhanced values to lower altitudes. We counter these distorted values by using non-zero a priori input in the lower thermosphere above 91 km.

Exactly as in the case of the MLT retrieval, we use SCIAMACHY's UV channel 1 (214–334 nm) to derive the NO number densities from atmospheric emissions of the NO gamma bands. Retrieving NO from the gamma band emissions was done previously in a variety of rocket (Cleary, 1986; Eparvier and Barth, 1992) and satellite (Frederick and Serafino, 1985; Barth et al., 2003; Minschwaner et al., 2004) experiments.

Further NO measurements in the mesosphere using different emissions were carried out, for example, using the Sub-Millimitre Radiometer (SMR) and the Optical Spectrograph and InfraRed Imaging System (OSIRIS) instruments on board the Odin satellite (Sheese et al., 2011, 2013). Infrared measurements we performed using the Atmospheric Chemistry Experiment Fourier transform spectrometer (ACE-FTS) on board SCISAT-1 (Kerzenmacher et al., 2008) and the Michelson Interferometer for Passive Atmospheric Sounding (MIPAS) also on the Envisat satellite (Funke et al., 2005; Bermejo-Pantaleón et al., 2011). More information about previous measurements of NO in the mesosphere can also be found in Bender et al. (2013).

This paper is organised as follows: we present some details about SCIAMACHY and its nominal limb mode in Sect. 2. Section 3 goes into detail about the retrieval method. Finally, we present our results and discuss the influence of different a priori choices in Sect. 4.

2 SCIAMACHY nominal mode

SCIAMACHY is a UV-vis-NIR (214–2380 nm) spectrometer on the European Envisat satellite. This satellite has been flying in a sun-synchronous orbit at approximately 800 km altitude since 2002 (Burrows et al., 1995; Bovensmann et al., 1999), but communication has been lost since April 2012. The main measurement modes include limb and nadir sounding as well as lunar and solar occultation measurements. Compared to the twice monthly driven MLT mode described in Bender et al. (2013); Langowski et al. (2014), the nominal limb scanning mode is one of the main measurement modes of SCIAMACHY and was performed almost daily for the almost ten years of successful operation. The nominal mode comprises limb scans from about -4 km up to 91 km which is just short of the maximum NO number density in the lower thermosphere. However, since this mode was carried out almost daily, it delivered a unique dataset of global continuous spectral measurements of the whole mesosphere.

From the beginning of its mission in August 2002 until the middle of October 2003, the nominal limb scans extended up to 105 km. On 15 October 2003, the sampling pattern of the nominal mode was changed to 30 limb tangent points from -4.5 km to about 91 km in approximately 3.3 km steps. The horizontal distance between the individual limb scans is about 7°–8°,

Atmos. Meas. Tech. Discuss., doi:10.5194/amt-2016-233, 2016
Manuscript under review for journal Atmos. Meas. Tech.
Published: 1 September 2016

Atmospheric Measurement Techniques Discussions

amounting to about 24 usable limb scans on the dayside of the orbit. More details about the measurement orbit sequence of SCIAMACHY can be found in Bovensmann et al. (1999).

As in the case of the SCIAMACHY MLT retrieval (Bender et al., 2013), we use the NO gamma bands for the retrieval. There, the first electronic state needs to be excited, restricting the useful measurements to times with available sunlight for this excitation.

3 Retrieval algorithm

The retrieval is adapted from the SCIAMACHY MLT NO retrieval, see Bender et al. (2013); Scharringhausen et al. (2008a, b); Langowski et al. (2014). We use the limb tangent point spectra from 50 km to the top at about 91 km. From these we fit the NO gamma bands (Eparvier and Barth, 1992; Stevens, 1995) to determine the NO slant column densities along the line of sight.

As discussed in Eparvier and Barth (1992); Stevens (1995); Bender et al. (2013), the NO gamma bands in the UV arise from an electronic transition where the first excited state $A^2\Sigma$ relaxes to the ground state $X^2\Pi$. Superposed on this electronic transition are the vibrational and rotational transitions, which constitute the different gamma bands.

The SCIAMACHY spectrometer resolves the vibrational lines but not the rotational lines. An example of a synthetic spectrum in the SCIAMACHY UV wavelength range can be found in Bender et al. (2013). As in the case of the MLT NO retrieval, we use the (0, 2), (1, 4), and (1, 5) vibrational transitions to retrieve the NO number densities from the nominal mode limb spectra. As discussed in Bender et al. (2013), the line of sight from the emission point to the satellite instrument is optically thin in these cases. An optically thin line of sight substantially decreases the computational effort for the forward model. Furthermore, we calculate the emissivities of the NO gamma bands with exactly the same parameters as given in Bender et al. (2013).

3.1 Radiative transfer

A generic objective in atmospheric remote sounding is to extract the relevant values (almost always at places without direct measurements) from the measured quantities. SCIAMACHY, and any limb sounder in general, measures the electromagnetic spectra reaching the instrument from along the line of sight through the atmosphere. In this study, we are interested in the NO number density distribution in the mesosphere.

The general forward model F relates measurements $\boldsymbol{y}$ to their depending unknown quantities $\boldsymbol{x}$ via

$$F : \text{unknowns} \rightarrow \text{measurements} , \quad \boldsymbol{x} \mapsto \boldsymbol{y} = F(\boldsymbol{x}) . \tag{1}$$

In general, the measured values are the spectral intensities at the satellite point. However, since we use non-resonant gamma transitions, these intensities are linearly related to the slant column densities (Bender et al., 2013). In our case, the measurements $\boldsymbol{y}$ are therefore given by the slant column densities from fitting the calculated NO gamma band spectra to the measured limb spectra. As noted above, we are interested in the number densities of NO at our self-defined retrieval grid point s, $\boldsymbol{x}(s)$.

Our forward model calculates the extinction along the line of sight from the tangent point to the satellite as well as along the line from the sun to the tangent point. Knowing the length of the line of sight within the grid cell, we then calculate the possible

Atmos. Meas. Tech. Discuss., doi:10.5194/amt-2016-233, 2016
Manuscript under review for journal Atmos. Meas. Tech.
Published: 1 September 2016

Atmospheric Measurement Techniques Discussions

Table 1. Regularisation parameters as used in the NO retrieval from SCIAMACHY limb scans.

λ_a	λ_{alt}	λ_{lat}
1×10^{-17}	3×10^{-17}	1×10^{-16}

emission signal from this cell. The details of this calculation are laid out in Scharringhausen et al. (2008b) and in Langowski et al. (2014).

We fit each vibrational NO gamma transition individually, which yields three separate values for the slant column densities and the fitting errors at the tangent points. Thus, $\boldsymbol{y} \in \mathbb{R}^{3N_{TP}}$ (with N_{TP} the number of tangent points) and is used in this way to retrieve the number densities $\boldsymbol{x}$.

The electronic excitation and emission occur at different wavelengths in general and for the three chosen gamma bands in particular. To account for this, we calculate the absorption matrix for the three gamma bands separately.

3.2 Retrieval algorithm

In our case, $\boldsymbol{x}$ and $\boldsymbol{y}$ in Eq. (1) have different dimensions, in particular, $\dim(\boldsymbol{x}) > \dim(\boldsymbol{y})$. Therefore, Eq. (1) can not be solved exactly because it has infinitely many solutions (assuming the system is consistent).

For one orbit, the SCIAMACHY MLT limb scans involve approximately $\dim(\boldsymbol{y}) \approx 25 \times 30 \times 3 = 2250$ measurements (limb scans per orbit $\times$ tangent points per limb scan $\times$ separate spectral fits). Whereas one orbit of SCIAMACHY nominal limb scans delivers $\dim(\boldsymbol{y}) \approx 25 \times 13 \times 3 = 975$ measurements above 50 km. The retrieval is done on a 2.5°$\times$ 2 km grid from 90°S to 90°N and from 60 km to 160 km. The grid size is $\dim(\boldsymbol{x}) = 72 \times 51 = 3672$ (latitude $\times$ altitude), clearly larger than $\dim(\boldsymbol{y})$.

Underdetermined systems can be solved using additional constraints, such as a priori input and regularisations (Rodgers, 1976; von Clarmann et al., 2003; Funke et al., 2005). Here we use both, that is, we use prior input and regularise vertically and horizontally. The a priori NO number densities are denoted by $\boldsymbol{x}_a$ and the accompanying covariance matrix by $\mathbf{S}_a$. We denote the regularisation matrices by $\mathbf{R}_{alt}$ and $\mathbf{R}_{lat}$, see Scharringhausen et al. (2008a); Langowski et al. (2014); Bender et al. (2013). We refer to Bender et al. (2013) for the exact details of how these are set up. The corresponding weighting parameters are again denoted by λ_a, λ_{alt}, and λ_{lat} for the a priori covariances, the vertical, and the horizontal regularisation; they are listed in Table 1[1].

The retrieval is equal to minimising the regularised χ^2:

$$\chi^2_{reg} = \|\mathbf{K}\boldsymbol{x} - \boldsymbol{y}\|^2_{S_y^{-1}} + \|\boldsymbol{x} - \boldsymbol{x}_a\|^2_{S_a^{-1}} \tag{2}$$

$$+ \lambda_{alt}\|\mathbf{R}_{alt}(\boldsymbol{x} - \boldsymbol{x}_a)\|^2 + \lambda_{lat}\|\mathbf{R}_{lat}(\boldsymbol{x} - \boldsymbol{x}_a)\|^2 , \tag{3}$$

[1]Note that because of improved so-called M-factors (a measure of the degradation of the SCIAMACHY detectors) and an adjusted fit error calculation, the numbers here differ from the ones given in (Bender et al., 2013).

Atmos. Meas. Tech. Discuss., doi:10.5194/amt-2016-233, 2016
Manuscript under review for journal Atmos. Meas. Tech.
Published: 1 September 2016

Atmospheric Measurement Techniques Discussions

where $\mathbf{K}$ is the Jacobian of Eq. (1). We minimise Eq. (2) with the same iterative algorithm as described in von Clarmann et al. (2003); Funke et al. (2005). The intermediate solution is given by

$$\boldsymbol{x}_{i+1} = \boldsymbol{x}_i + \left(\mathbf{K}^T\mathbf{S}_y^{-1}\mathbf{K} + \mathbf{R}\right)^{-1} \tag{4}$$

$$\cdot \left[\mathbf{K}^T\mathbf{S}_y^{-1}(\boldsymbol{y} - \boldsymbol{y}_i(\boldsymbol{x}_i)) + \mathbf{R}(\boldsymbol{x}_\mathrm{a} - \boldsymbol{x}_i)\right] , \tag{5}$$

with the regularisation matrix $\mathbf{R}$ defined as

$$\mathbf{R} := \mathbf{S}_\mathrm{a}^{-1} + \lambda_\mathrm{alt}\mathbf{R}_\mathrm{alt}^T\mathbf{R}_\mathrm{alt} + \lambda_\mathrm{lat}\mathbf{R}_\mathrm{lat}^T\mathbf{R}_\mathrm{lat} . \tag{6}$$

3.3 A priori setup

The SCIAMACHY nominal limb scans extend only up to ≈91 km in altitude, but the maximal NO density is located between 100 km and 110 km in polar regions (Barth et al., 2003; Marsh et al., 2004; Funke et al., 2005; Bender et al., 2015). This maximal density lies along the line of sight of the instrument but it is not explicitly resolved with dedicated limb tangent points. Retrieving the NO number densities up to 160 km, this adversely affects all values, in particular below 100 km. Using a priori input to model these maximal values in the lower thermosphere is therefore crucial to get correct number densities, also below 100 km.

In this work, we use two models of the NO number density in the thermosphere. The first is the NOEM model (Marsh et al., 2004), an empirical model based on SNOE observations (Barth et al., 2003). This model is also used as a priori input for the MIPAS NO retrievals (Funke et al., 2005). It is, however, constructed only for altitudes from 100 km to 150 km (Marsh et al., 2004) and set to constant below 100 km.

The second model uses results from the multi-linear regression analysis from the measurement comparison study of NO from four instruments: ACE-FTS, MIPAS, SCIAMACHY, and SMR (Bender et al., 2015). Here we use the parameters from the regression fit from 94 km to 150 km of the composite data set.

At 92 km and below, the a priori is set equal to zero with a smooth transition between 100 km and 92 km. For the smooth transition we use the standard analysis approach for the partition of unity. First, we define the smooth function $\theta(t)$ by

$$\theta(t) := \begin{cases} 0 , & t \leq 0 \\ \mathrm{e}^{-1/t} , & t > 0 \end{cases} , \tag{7}$$

and the smooth transition $\phi(s)$ from zero to one by

$$\phi(s) := \frac{\theta(s)}{\theta(s) + \theta(1-s)} = \begin{cases} 0 , & s \leq 0 \\ 1 , & s \geq 1 \end{cases} . \tag{8}$$

Note that $\phi(s)$ is smooth for all $s \in \mathbb{R}$. Then a smooth transition from one at altitude a to zero at and below $a - w$ is given by scaling the argument of ϕ in the following way:

$$\Phi(s, a, w) := \phi\left(\frac{s - a + w}{w}\right) = \begin{cases} 0 , & s \leq a - w \\ 1 , & s \geq a \end{cases} . \tag{9}$$

Atmos. Meas. Tech. Discuss., doi:10.5194/amt-2016-233, 2016
Manuscript under review for journal Atmos. Meas. Tech.
Published: 1 September 2016

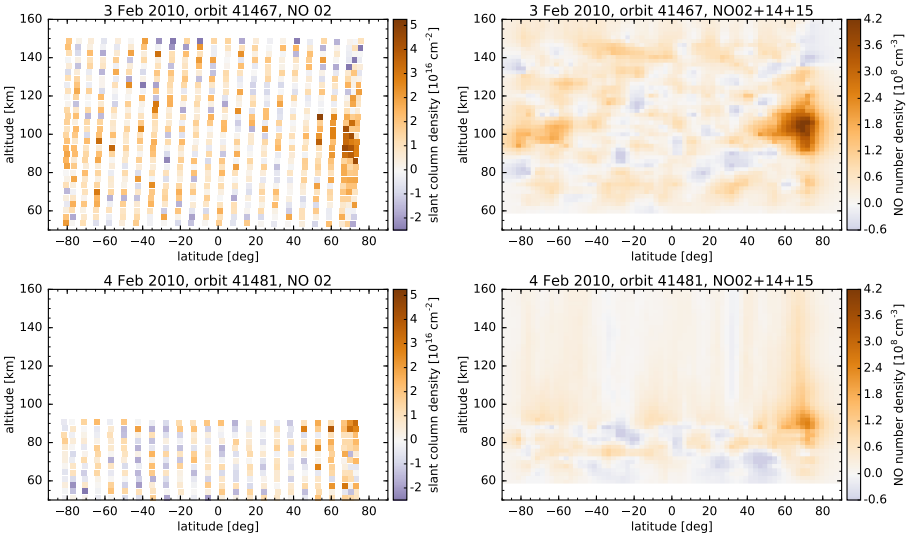

Figure 1. NO slant column densites (left column) and number densities (right column) along one SCIAMACHY MLT orbit (no. 41467, 3 February 2010, top row) and one nominal orbit (no. 41481, 4 February 2010, bottom row).

We eventually scale the a priori input x_a by $\Phi(s, a, w)$ with $a = 100$ km and $w = 8$ km.

3.4 Further model input

Furthermore, as described in Bender et al. (2013), the atmospheric temperatures are needed to calculate the emissivity of the NO transitions. We use the NRLMSISE-00 model (Picone et al., 2002) which derives the temperatures using the geomagnetic A_p index and the solar radio flux $f_{10.7}$. Both are taken as daily values from the Space Physics Interactive Data Resource (SPIDR) service (NGDC and NOAA, 2011) of the National Geophysical Data Center (NGDC) of the National Oceanic and Atmospheric Administration (NOAA).

4 Results

4.1 NO number density

Equivalently to the MLT retrieval described in Bender et al. (2013), we present the individual steps of the retrieval. We take a detailed look at the same sample orbit, number 41467 from 3 February 2010. The upper left panel of Fig. 1 shows the fitted (0, 2) slant column densities at all tangent points of the example MLT orbit. As discussed in Bender et al. (2013), the region of largest slant column densities lies between 60°N and 70°N around 100 km.

Accordingly, using the MLT retrieval algorithm without a priori, the retrieved NO number densities for this example orbit are shown in the upper right panel of Fig. 1. In addition to the expected high-density region in the Northern Hemisphere, between

Atmos. Meas. Tech. Discuss., doi:10.5194/amt-2016-233, 2016
Manuscript under review for journal Atmos. Meas. Tech.
Published: 1 September 2016

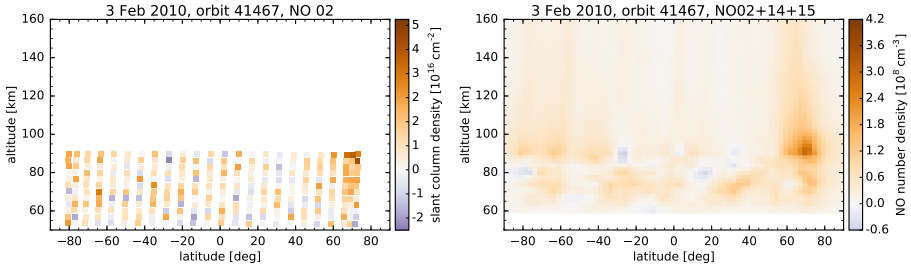

Figure 2. Results from the SCIAMACHY MLT sample orbit (no. 41467, 3 February 2010) restricted to the 50–91 km limb tangent points. NO slant column densities for the (0, 2) transition (left) and the retrieved NO number densities without a priori (right).

55°N and 75°N and around 105 km, we also observe enhanced number densities in the Southern Hemisphere. There we find higher values between 55°S and 85°S around 100 km.

In contrast to that, the lower left panel of Fig. 1 shows the slant column densities of a sample orbit containing nominal limb scans (no. 41481 from 4 February 2010). We chose this particular orbit because it covers approximately the same longitude as the chosen MLT orbit above, but on the following day. As discussed above, the highest tangent point lies at about 91 km which manifests in much shorter columns in the lower left panel of Fig. 1 compared to the upper left panel of the same figure. Furthermore, the order of the nominal limb scans are opposite to the MLT limb scan order, from bottom to top (nominal) instead of from top to bottom (MLT). This results in an opposite slope of the slant column densities per limb scan because the satellite moves from North to South during one scan. For the retrieval, however, this change is irrelevant since we calculate the path lengths through the atmosphere from the actual tangent points.

The retrieved NO number densities from these slant column densities are shown in the lower right panel of Fig. 1. Since we extend the retrieval up to 160 km to be directly comparable to the MLT limb scans, values above about 91 km smoothly extend upwards. This is a direct consequence of the regularisation we use. In general, the number densities are smaller then from the MLT orbit the day before. We assume that these lower values are related to the large natural variability of NO in the mesosphere.

4.2 Simulation of nominal mode

SCIAMACHY's MLT mode and nominal mode were carried out on different days. Therefore, we cannot directly compare the number densities from both modes. To estimate the error introduced by sampling only up to 91 km instead of 150 km, we simulate the nominal mode on MLT days by restricting the limb scan data from the MLT mode to 91 km before we do the retrieval. We then compare the resulting number densities over the full altitude range. However, when evaluating the results the main focus should lie on altitudes below 91 km. We start this comparison without a priori input and evaluate the effect of the different prior choices below in Sect. 4.3.

The restricted slant column densities are shown in the left panel of Fig. 2. The retrieved NO number densities from these slant column densities are shown in the right panel of Fig. 2.

Atmos. Meas. Tech. Discuss., doi:10.5194/amt-2016-233, 2016
Manuscript under review for journal Atmos. Meas. Tech.
Published: 1 September 2016

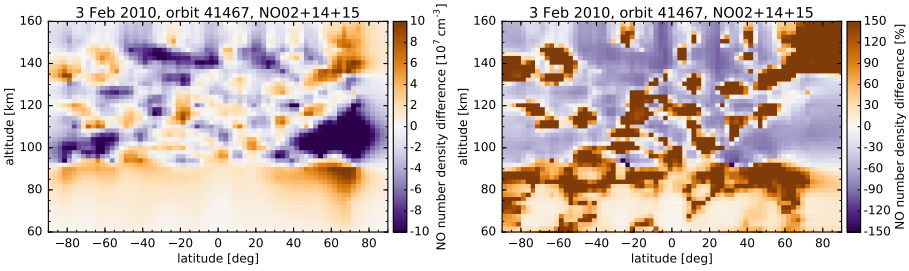

Figure 3. Absolute NO number density differences (left) and relative differences (right) from the SCIAMACHY MLT mode limb scans restricted to 50–91 km and zero a priori compared to the full retrieval (sample orbit no. 41467, 3 February 2010).

Figure 3 shows the absolute (left panel) and relative (right panel) differences of the retrieved NO number densities compared to the full MLT retrieval. The differences are mostly negative above 91 km because there we have no slant column densities from dedicated limb tangent points. Equivalently, the differences are positive below this altitude for the same reason: we incorrectly attribute the measured slant column densities to NO number densities at lower altitudes. The sometimes large relative differences should not be over-interpreted because at places with low number densities, large relative differences occur easily.

4.3 A priori influence

As seen in Fig. 3, omitting the dedicated limb tangent points above 91 km enhances the retrieved NO number densities below about 91 km. To compensate these enhanced values, we used non-zero a priori input to model the NO number density above 100 km, as described in Sect. 3.3. The a priori input from the NOEM model (Marsh et al., 2004) is shown in the upper left panel of Fig. 4 for the chosen example orbit. Similar, the input from the regression model is shown in the lower left panel of Fig. 4.

Including these prior inputs, the retrieved NO number densities from the restricted MLT limb scans are shown in the right column of Fig. 4. In particular, we present the results using the NOEM model in the upper right panel and using the regression a priori in the lower right panel.

Figure 5 shows the relative differences of the retrieved NO number densities from the restricted MLT limb scans compared to the full MLT retrieval results, this time using a priori input (compare to Fig. 3). In the first figure we used the NOEM model input above 100 km, and in the second case the input is derived from the regression analysis (Bender et al., 2015).

Figure 5 gives only a rough qualitative look at the differences between the MLT number densities and the densities when we restrict the MLT limb scans to 91 km. To assess the differences quantitatively, we calculate the differences of the respective daily zonal mean number densities for all SCIAMACHY MLT measurement days. In particular, we compare the daily mean number densities in three latitude bands: 90°S–50°S, 50°S–50°N, and 50°N–90°N.

The median of the number densities retrieved from the restricted MLT scans in these three latitude bands compared to the results from the full MLT retrieval are shown in the top panel of Fig. 6. As before we find that restricting the covered altitude range to 91 km results in overestimating the number densities between 70 km and 91 km. Using either a priori input underestimates the number densities in that altitude region, more severely when using the NOEM model.

Atmos. Meas. Tech. Discuss., doi:10.5194/amt-2016-233, 2016
Manuscript under review for journal Atmos. Meas. Tech.
Published: 1 September 2016

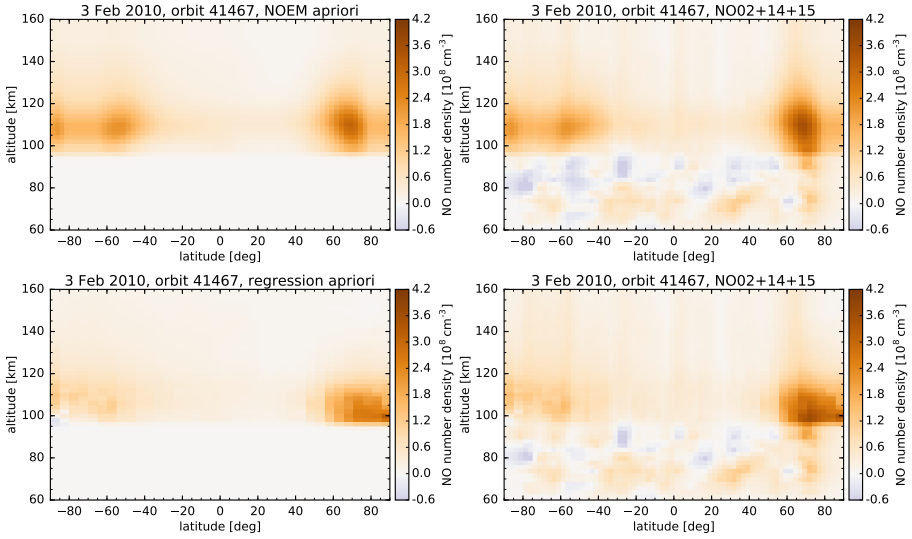

Figure 4. NO number density a priori input from the NOEM model (upper left) and the regression model (lower left). Retrieved NO number densities from the limited SCIAMACHY MLT limb scans using the NOEM model (upper right) and the regression model (lower right) a priori (sample orbit no. 41467, 3 February 2010).

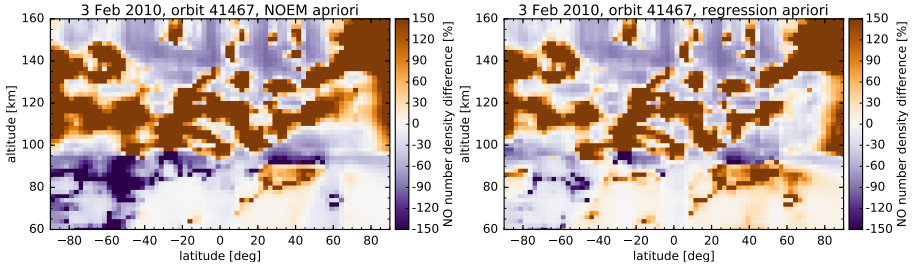

Figure 5. Relative NO number density differences from the SCIAMACHY MLT mode limb scans restricted to 50–91 km using the NOEM model (right) and the regression model (left) as a priori input compared to the full retrieval (sample orbit no. 41467, 3 February 2010).

The median of the absolute differences of the number densities of restricted MLT scans to the results from the full MLT retrieval are shown in the middle panel of Fig. 6. The bottom panel of Fig. 6 shows the median of the corresponding relative differences to illustrate the effect of the different a priori inputs.

In the following we concentrate on the differences between 60 km and 91 km. We find that without a priori input (light blue line in Fig. 6), at the top most altitude (91 km) the retrieved number densities are up to 1×10^7 cm^{-3} (middle and low latitudes) and up to 2×10^7 cm^{-3} larger (high latitudes). In all three region, this corresponds to about 100%. Below about 80 km at high latitudes, the difference is smaller than 1×10^7 cm^{-3}, which translates to about 50%. At middle and low latitudes, the absolute

Atmos. Meas. Tech. Discuss., doi:10.5194/amt-2016-233, 2016
Manuscript under review for journal Atmos. Meas. Tech.
Published: 1 September 2016

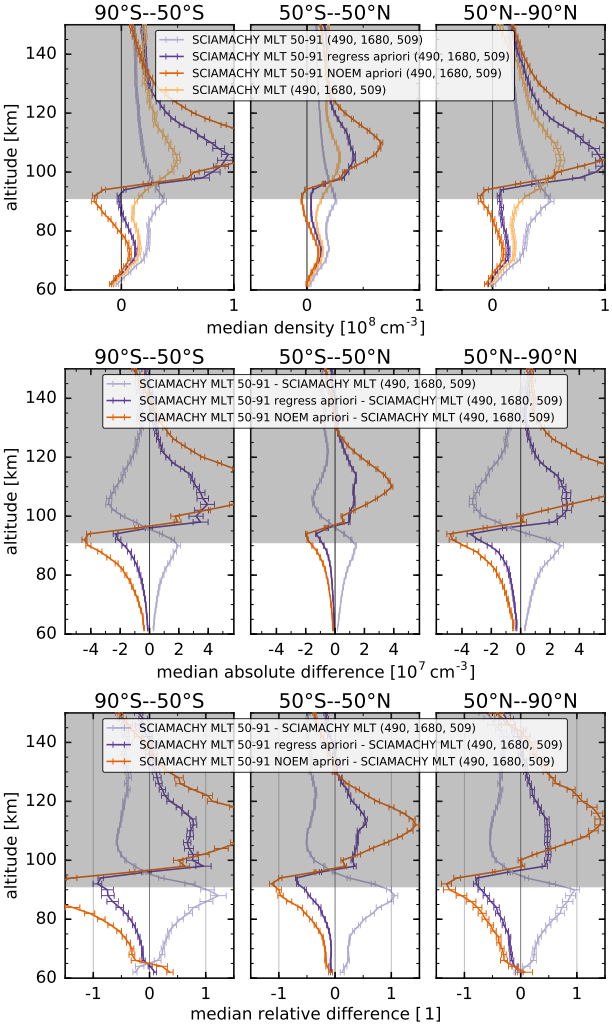

Figure 6. Median of the NO number densities (top) as well as the absolute (middle) and relative (bottom) differences to the full MLT retrieval in three latitude bands. The results are shown for the restricted (50–91 km) MLT scans without a priori input (light purple), and using the two a priori choices (dark purple: regression model, dark orange: NOEM model). The number densities from the full SCIAMACHY MLT scans are shown in light orange.

differences drop to about 0.5×10^7 cm^{-3} at 80 km, which is equally about 50%. Below 70 km, the differences drop further, to below about 25% in all regions.

Using a priori inputs (orange and purple lines in Fig. 6) gives smaller number densities below 91 km in general. Compared to the full MLT retrieval, using the NOEM model (orange line in those figures) has the largest effect with 5×10^7 cm^{-3} ($> 100\%$) smaller number densities at high latitudes at 91 km. Below 80 km in these regions, the difference drops to about -2×10^7 cm^{-3} ($\approx$ -50%) and further to -1×10^7 cm^{-3} ($\approx$ -30%) below 70 km. At middle and low latitudes, the largest difference is about

Atmos. Meas. Tech. Discuss., doi:10.5194/amt-2016-233, 2016
Manuscript under review for journal Atmos. Meas. Tech.
Published: 1 September 2016

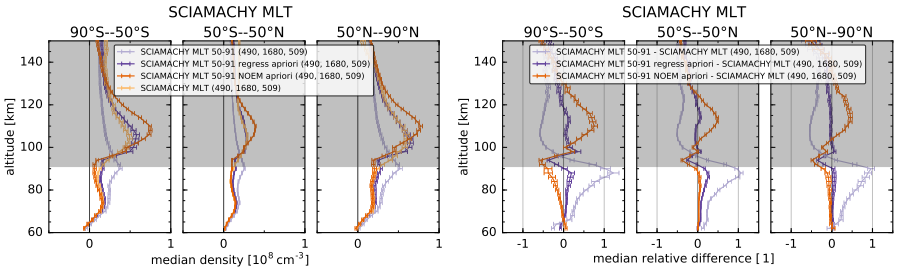

Figure 7. Median of the NO number densities (left) and the relative differences (right) using half the a priori values compared to the full SCIAMACHY MLT limb scans number densities.

-2×10^7 cm^{-3} (≈ -100%) at 91 km. Below 80 km in that region, the difference declines to less than about -1×10^7 cm^{-3} (≈ -50%), and below 70 km further to about -0.5×10^7 cm^{-3} (≈ -20%)

Using the regression model as a priori input (purple line), these differences are smaller. At high latitudes, the largest difference is -3×10^7 cm^{-3} (-90% to -100%) at 91 km, dropping to less than -1×10^7 cm^{-3} (-50%) below about 80 km. Below 70 km at hight latitudes, the differences become smaller than about -0.5×10^7 cm^{-3} (-20%). At middle and low latitudes, the largest difference is approximately -1×10^7 cm^{-3} (-60%) at 91 km, declining to less than -0.25×10^7 cm^{-3} (-20%) below 80 km. Below 70 km in this region, the relative difference is smaller than -10%.

Since using the a priori values seem to over-correct the missing data above 100 km, we chose to also analyse the results using only half the a priori values. For the NOEM model, this is justified by the origin of the model. Marsh et al. (2004) used the data from the SNOE experiment (Barth et al., 2003) to construct the NOEM model using empirical orthogonal functions. The SNOE experiment itself was carried out during elevated solar activity, which may have resulted in larger NO number densities in the MLT region compared to lower solar activity. This was also observed in Bender et al. (2013), where the NOEM model overestimates the number densities compared to the MIPAS and SCIAMACHY measurements, in particular at times of low solar activity (see Figs. 13 and 14 in Bender et al. (2013)).

The median of the number densities of the restricted MLT scans using half the a priori values compared to the number densities from the full MLT retrieval are shown in the left panel of Fig. 7. Using half the model number densities as a priori input brings the results much closer together between 60 km and 80 km in all three regions. Some differences remain between 80 km and 91 km at high southern latitudes, in particular when using (half of) the NOEM model as a priori input. The right panel of Fig. 7 shows the corresponding median of the relative differences.

At high northern latitudes, using half the values of either model as a priori results in number densities differences less than 6% below 80 km, and less than 10% above. Using half the NOEM model at middle and low latitudes results in less than 6% differences across the altitude range of interest, whereas using half the regression model results in about 10% at 80 km and 20% larger number densities at 91 km. At high southern latitudes, the differences using half the NOEM model are largest, up to -40% at the top and up to -20% at 80 km but around ±4% below 70 km. Using the regression model here leads to about the same differences as at middle and low latitudes. We summarise our findings regarding the different a priori choices in Tab. 2.

Atmos. Meas. Tech. Discuss., doi:10.5194/amt-2016-233, 2016
Manuscript under review for journal Atmos. Meas. Tech.
Published: 1 September 2016

Atmospheric Measurement Techniques Discussions

Table 2. Differences of the NO number densities using the different a priori choice compared to the full MLT limb scan retrieved values. NH and SH indicate exceptions at high northern and high southern latitudes.

altitude range	zero	NOEM	regression	half NOEM	half regression
80–91 km	50...100%	-60...<-100%	-35...-100%	< ±10%, -20...-40% (SH)	10...20%, ≈6% (NH)
70–80 km	25...50%	-30...-60%	-20...-35%	< ±6%, -5...-20% (SH)	5...10%, 3...5% (NH)
< 70 km	< 25%	> -30%	> -20%	< ±4%	3...7%, < 3% (NH)

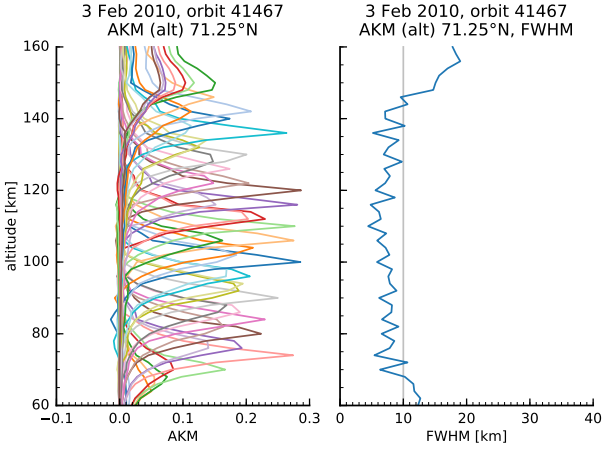

Figure 8. Altitude averaging kernel matrix elements (left panel) for a sample orbit (no. 41467, 3 February 2010) at a particular latitude grid point (71.25°N). Corresponding full width at half maximum values (right panel) at the same location.

4.4 Resolution

The vertical resolution using the SCIAMACHY MLT scans was extensively discussed in Bender et al. (2013). Here we briefly review the main results. The vertical averaging kernel elements of the MLT retrieval for the chosen example orbit are shown in the left panel of Fig. 8. As a measure of the vertical resolution, the corresponding full widths at half maximum (fwhm) are shown in the right panel of Fig. 8. From 70 km to about 140 km, the vertical resolution is about 10 km or better.

Figure 9 (first panel from the left) shows the averaging kernel matrix elements from an example nominal mode orbit (no. 41481 from 4 February 2010). The second panel in the same figure shows the vertical resolution given by the full width at half maximum of those line sums. The resolution is about 10 km or better between about 65 km and 90 km and sharply decreases above 90 km. This is to be expected because we have only column information above 91 km from the nominal mode limb scans.

For comparison, the third and fourth panel of Fig. 9 show the averaging kernel matrix elements and their full widths at half maximum from restricting the MLT limb scans to 91 km. Between 60 km and 90 km, the resolution resembles that of the full MLT scan shown in Fig. 8. The sharp drop in vertical resolution is directly related to the missing information above 91 km.

Atmos. Meas. Tech. Discuss., doi:10.5194/amt-2016-233, 2016
Manuscript under review for journal Atmos. Meas. Tech.
Published: 1 September 2016

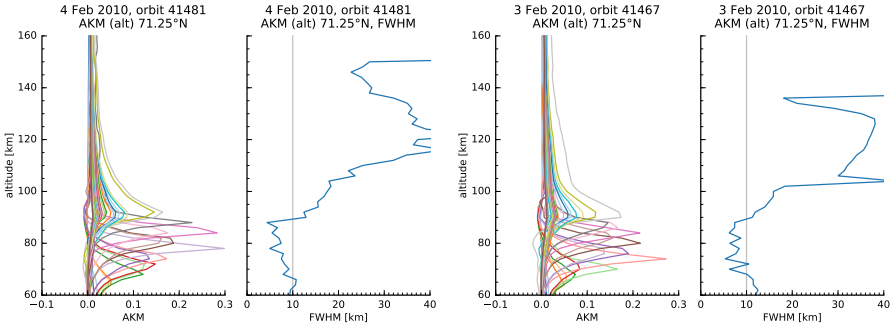

Figure 9. Altitude averaging kernel matrix elements (first panel from the left) and the respective full widths at half maximum (second panel) at the 71.25°N latitude bin for the sample nominal mode orbit (no. 41481, 4 February 2010). For comparison, the averaging kernel matrix elements from the retrieval of the MLT scan limited to below 91 km and the full width at half maximum resolution at the same latitude bin of the sample MLT orbit are shown in the right two panels (sample orbit no. 41467, 3 February 2010).

5 Conclusions

We present an algorithm to retrieve NO number densities in the mesosphere from measured scattered solar radiation and atmospheric emissions in limb viewing geometry from the SCIAMACHY instrument on Envisat. We apply the method developed for SCIAMACHY's special MLT limb scans (50–150 km, Bender et al. (2013)) to SCIAMACHY's nominal limb scans (-3–91 km).

The altitude range of meaningful results from the SCIAMACHY nominal limb scans extends from 60 km to about 85 km. We find that the missing measurements above about 91 km manifest in larger NO number densities below 91 km if no prior input is used. Including a priori input in the retrieval leads to smaller number densities below 91 km for both our a priori choices, the NOEM model (Marsh et al., 2004) and the multi-linear regression result from Bender et al. (2015). However, we find that using half the model inputs as a priori recovers the values below 91 km within 40% and below 80 km within 20% or better. Taking into account that the regression model already includes the SCIAMACHY MLT data, it should be used with caution. We therefore recommend using half of the NOEM model values as prior input for the retrieval as currently the best option. Unfortunately, comparisons between our NO data products and NO data products from other instruments are limited. The reason is that the sensitive altitude ranges are different, too low in some cases (e.g., Odin/SMR > 85 km) or too high in other cases (e.g., MIPAS nominal mode < 60 km).

The SCIAMACHY nominal limb scans provide almost ten years continuous daily spectra of the middle atmosphere (up to ≈ 90 km). Retrieving NO from these spectra is an important key in connecting solar activity to middle atmosphere composition and dynamics. Solar-wind and auroral particles precipitating into the upper atmosphere produce NO which is reduced via photolysis by solar UV radiation. Therefore, NO lives long in polar winter at auroral latitudes without direct sunlight. This allows NO to be transported down, sometimes to the stratosphere where it affects the polar ozone layer.

Atmos. Meas. Tech. Discuss., doi:10.5194/amt-2016-233, 2016
Manuscript under review for journal Atmos. Meas. Tech.
Published: 1 September 2016

Atmospheric Measurement Techniques Discussions

The ten years daily measurements allow to study NO in the mesosphere with respect to long-term (years) and short-term (days) variations of solar activity (Sinnhuber et al., 2016). In particular, it is a start to quantify the production rate and lifetime of particle-produced NO in these regions. Further work is planned to use this ten-year dataset to constrain mesosphere NO in chemistry climate models as an important aspect of solar influence on climate.

Acknowledgements. S.B. and M.S. thank the Helmholtz-society for funding this project under the grant number VH-NG-624. The SCIAMACHY project was funded by German Aerospace (DLR), the Dutch Space Agency, SNO, and the Belgium ministry. ESA funded the Envisat project. The University of Bremen as Principal Investigator has led the scientific support and development of SCIAMACHY and the scientific exploitation of its data products. We acknowledge support by Deutsche Forschungsgemeinschaft and Open Access Publishing Fund of Karlsruhe Institute of Technology.

Atmos. Meas. Tech. Discuss., doi:10.5194/amt-2016-233, 2016
Manuscript under review for journal Atmos. Meas. Tech.
Published: 1 September 2016

Atmospheric Measurement Techniques Discussions

References

Barth, C. A., Mankoff, K. D., Bailey, S. M., and Solomon, S. C.: Global observations of nitric oxide in the thermosphere, J. Geophys. Res., 108, 1027, doi:10.1029/2002JA009458, 2003.

Bender, S., Sinnhuber, M., Burrows, J. P., Langowski, M., Funke, B., and López-Puertas, M.: Retrieval of nitric oxide in the mesosphere and lower thermosphere from SCIAMACHY limb spectra, Atmos. Meas. Tech., 6, 2521–2531, doi:10.5194/amt-6-2521-2013, http://www.atmos-meas-tech.net/6/2521/2013/, 2013.

Bender, S., Sinnhuber, M., von Clarmann, T., Stiller, G., Funke, B., López-Puertas, M., Urban, J., Pérot, K., Walker, K. A., and Burrows, J. P.: Comparison of nitric oxide measurements in the mesosphere and lower thermosphere from ACE-FTS, MIPAS, SCIAMACHY, and SMR, Atmos. Meas. Tech., 8, 4171–4195, doi:10.5194/amt-8-4171-2015, http://www.atmos-meas-tech.net/8/4171/2015/, 2015.

Bermejo-Pantaleón, D., Funke, B., López-Puertas, M., García-Comas, M., Stiller, G. P., von Clarmann, T., Linden, A., Grabowski, U., Höpfner, M., Kiefer, M., Glatthor, N., Kellmann, S., and Lu, G.: Global observations of thermospheric temperature and nitric oxide from MIPAS spectra at 5.3 µm, J. Geophys. Res., 116, A10313, doi:10.1029/2011JA016752, 2011.

Bovensmann, H., Burrows, J. P., Buchwitz, M., Frerick, J., Noël, S., Rozanov, V. V., Chance, K. V., and Goede, A. P. H.: SCIAMACHY: Mission Objectives and Measurement Modes, J. Atmos. Sci., 56, 127–150, doi:10.1175/1520-0469(1999)056<0127:SMOAMM>2.0.CO;2, 1999.

Burrows, J. P., Hölzle, E., Goede, A. P. H., Visser, H., and Fricke, W.: SCIAMACHY – scanning imaging absorption spectrometer for atmospheric chartography, Acta Astronaut., 35, 445–451, doi:10.1016/0094-5765(94)00278-T, http://www.sciencedirect.com/science/article/pii/009457659400278T, 1995.

Cleary, D. D.: Daytime High-Latitude Rocket Observations of the NO γ, δ, and ε Bands, J. Geophys. Res., 91, 11337–11344, doi:10.1029/JA091iA10p11337, 1986.

Eparvier, F. G. and Barth, C. A.: Self-Absorption Theory Applied to Rocket Measurements of the Nitric Oxide (1, 0) γ Band in the Daytime Thermosphere, J. Geophys. Res., 97, 13723–13731, doi:10.1029/92JA00993, 1992.

Frederick, J. E. and Serafino, G. N.: Satellite observations of the nitric oxide dayglow: Implications for the behavior of mesospheric and lower-thermospheric odd nitrogen, J. Geophys. Res., 90, 3821–3830, doi:10.1029/JD090iD02p03821, 1985.

Funke, B., López-Puertas, M., von Clarmann, T., Stiller, G. P., Fischer, H., Glatthor, N., Grabowski, U., Höpfner, M., Kellmann, S., Kiefer, M., Linden, A., Mengistu Tsidu, G., Milz, M., Steck, T., and Wang, D. Y.: Retrieval of stratospheric NOx from 5.3 and 6.2 µm nonlocal thermodynamic equilibrium emissions measured by Michelson Interferometer for Passive Atmospheric Sounding (MIPAS) on Envisat, J. Geophys. Res., 110, D09302, doi:10.1029/2004JD005225, 2005.

Hendrickx, K., Megner, L., Gumbel, J., Siskind, D. E., Orsolini, Y. J., Tyssøy, H. N., and Hervig, M.: Observation of 27 day solar cycles in the production and mesospheric descent of EPP-produced NO, J. Geophys. Res., 120, 8978–8988, doi:10.1002/2015JA021441, 2015JA021441, 2015.

Kerzenmacher, T., Wolff, M. A., Strong, K., Dupuy, E., Walker, K. A., Amekudzi, L. K., Batchelor, R. L., Bernath, P. F., Berthet, G., Blumenstock, T., Boone, C. D., Bramstedt, K., Brogniez, C., Brohede, S., Burrows, J. P., Catoire, V., Dodion, J., Drummond, J. R., Dufour, D. G., Funke, B., Fussen, D., Goutail, F., Griffith, D. W. T., Haley, C. S., Hendrick, F., Höpfner, M., Huret, N., Jones, N., Kar, J., Kramer, I., Llewellyn, E. J., López-Puertas, M., Manney, G., McElroy, C. T., McLinden, C. A., Melo, S., Mikuteit, S., Murtagh, D., Nichitiu, F., Notholt, J., Nowlan, C., Piccolo, C., Pommereau, J.-P., Randall, C., Raspollini, P., Ridolfi, M., Richter, A., Schneider, M., Schrems, O., Silicani, M., Stiller, G. P., Taylor, J., Tétard, C., Toohey, M., Vanhellemont, F., Warneke, T., Zawodny, J. M., and Zou, J.: Validation of

NO_2 and NO from the Atmospheric Chemistry Experiment (ACE), Atmos. Chem. Phys., 8, 5801–5841, doi:10.5194/acp-8-5801-2008, http://www.atmos-chem-phys.net/8/5801/2008/, 2008.

Langowski, M., Sinnhuber, M., Aikin, A. C., von Savigny, C., and Burrows, J. P.: Retrieval algorithm for densities of mesospheric and lower thermospheric metal atom and ion species from satellite-borne limb emission signals, Atmos. Meas. Tech., 7, 29–48, doi:10.5194/amt-7-29-2014, http://www.atmos-meas-tech.net/7/29/2014/, 2014.

Maliniemi, V., Asikainen, T., and Mursula, K.: Spatial distribution of Northern Hemisphere winter temperatures during different phases of the solar cycle, J. Geophys. Res., 119, 9752–9764, doi:10.1002/2013JD021343, 2014.

Marsh, D. R., Solomon, S. C., and Reynolds, A. E.: Empirical model of nitric oxide in the lower thermosphere, J. Geophys. Res., 109, A07301, doi:10.1029/2003JA010199, 2004.

Minschwaner, K., Bishop, J., Budzien, S. A., Dymond, K. F., Siskind, D. E., Stevens, M. H., and McCoy, R. P.: Middle and upper thermospheric odd nitrogen: 2. Measurements of nitric oxide from Ionospheric Spectroscopy and Atmospheric Chemistry (ISAAC) satellite observations of NO γ band emission, J. Geophys. Res., 109, A01304, doi:10.1029/2003JA009941, 2004.

NGDC and NOAA: Space Physics Interactive Data Resource (SPIDR), http://spidr.ngdc.noaa.gov/spidr/, [Online; accessed 11-Dec-2013], 2011.

Picone, J. M., Hedin, A. E., Drob, D. P., and Aikin, A. C.: NRLMSISE-00 empirical model of the atmosphere: Statistical comparisons and scientific issues, J. Geophys. Res., 107, 1468, doi:10.1029/2002JA009430, 2002.

Rodgers, C. D.: Retrieval of atmospheric temperature and composition from remote measurements of thermal radiation, Rev. Geophys., 14, 609–624, doi:10.1029/RG014i004p00609, 1976.

Scharringhausen, M., Aikin, A. C., Burrows, J. P., and Sinnhuber, M.: Global column density retrievals of mesospheric and thermospheric MgI and MgII from SCIAMACHY limb and nadir radiance data, J. Geophys. Res., 113, D13303, doi:10.1029/2007JD009043, WOS:000257797900001, 2008a.

Scharringhausen, M., Aikin, A. C., Burrows, J. P., and Sinnhuber, M.: Space-borne measurements of mesospheric magnesium species – a retrieval algorithm and preliminary profiles, Atmos. Chem. Phys., 8, 1963–1983, doi:10.5194/acp-8-1963-2008, http://www.atmos-chem-phys.net/8/1963/2008/, 2008b.

Seppälä, A., Randall, C. E., Clilverd, M. A., Rozanov, E., and Rodger, C. J.: Geomagnetic activity and polar surface air temperature variability, J. Geophys. Res., 114, n/a–n/a, doi:10.1029/2008JA014029, a10312, 2009.

Seppälä, A., Clilverd, M. A., Beharrell, M. J., Rodger, C. J., Verronen, P. T., Andersson, M. E., and Newnham, D. A.: Substorm-induced energetic electron precipitation: Impact on atmospheric chemistry, Geophys. Res. Lett., 42, 8172–8176, doi:10.1002/2015GL065523, 2015GL065523, 2015.

Sheese, P. E., Gattinger, R. L., Llewellyn, E. J., Boone, C. D., and Strong, K.: Nighttime nitric oxide densities in the Southern Hemisphere mesosphere–lower thermosphere, Geophys. Res. Lett., 38, n/a–n/a, doi:10.1029/2011GL048054, 2011.

Sheese, P. E., Strong, K., Gattinger, R. L., Llewellyn, E. J., Urban, J., Boone, C. D., and Smith, A. K.: Odin observations of Antarctic nighttime NO densities in the mesosphere-lower thermosphere and observations of a lower NO layer, J. Geophys. Res., 118, 7414–7425, doi:10.1002/jgrd.50563, 2013.

Sinnhuber, M., Nieder, H., and Wieters, N.: Energetic Particle Precipitation and the Chemistry of the Mesosphere/Lower Thermosphere, Surv. Geophys., 33, 1281–1334, doi:10.1007/s10712-012-9201-3, 2012.

Sinnhuber, M., Friederich, F., Bender, S., and Burrows, J. P.: The response of mesospheric NO to geomagnetic forcing in 2002–2012 as seen by SCIAMACHY, J. Geophys. Res., pp. n/a–n/a, doi:10.1002/2015JA022284, http://onlinelibrary.wiley.com/doi/10.1002/2015JA022284/abstract, 2015JA022284, 2016.

Stevens, M. H.: Nitric Oxide γ Band Fluorescent Scattering and Self-Absorption in the Mesosphere and Lower Thermosphere, J. Geophys. Res., 100, 14735–14742, doi:10.1029/95JA01616, 1995.

Verronen, P. T. and Lehmann, R.: Enhancement of odd nitrogen modifies mesospheric ozone chemistry during polar winter, Geophys. Res. Lett., 42, 10,445–10,452, doi:10.1002/2015GL066703, 2015GL066703, 2015.

von Clarmann, T., Glatthor, N., Grabowski, U., Höpfner, M., Kellmann, S., Kiefer, M., Linden, A., Tsidu, G. M., Milz, M., Steck, T., Stiller, G. P., Wang, D. Y., Fischer, H., Funke, B., Gil-López, S., and López-Puertas, M.: Retrieval of temperature and tangent altitude pointing from limb emission spectra recorded from space by the Michelson Interferometer for Passive Atmospheric Sounding (MIPAS), J. Geophys. Res., 108, 4736, doi:10.1029/2003JD003602, 2003.